

High-energy neutrino emission associated with gravitational-wave signals: effects of cocoon photons and constraints on late-time emission

RIKI MATSUI ¹, SHIGEO S. KIMURA ^{2,1}, KENJI TOMA ^{2,1} AND KOHTA MURASE ^{3,4,5}

¹*Astronomical Institute, Graduate School of Science, Tohoku University, Sendai 980-8578, Japan*

²*Frontier Research Institute for Interdisciplinary Sciences, Tohoku University, Sendai 980-8578, Japan*

³*Department of Physics; Department of Astronomy and Astrophysics; Center for Multimessenger Astrophysics, Institute for Gravitation and the Cosmos, The Pennsylvania State University, University Park, Pennsylvania 16802, USA*

⁴*School of Natural Sciences, Institute for Advanced Study,*

⁵*Center for Gravitational Physics and Quantum Information, Yukawa Institute for Theoretical Physics, Kyoto University, Kyoto, Kyoto 606-8502, Japan*

ABSTRACT

We investigate prospects for the detection of high-energy neutrinos produced in the prolonged jets of short gamma-ray bursts (sGRBs). The X-ray lightcurves of sGRBs show extended emission components lasting for 100-1000 seconds, which are considered to be produced by prolonged engine activity. Jets by prolonged engine activity should interact with photons in the cocoon formed by the jet propagation inside the ejecta of neutron star mergers. We calculate neutrino emission from jets by prolonged engine activity, taking account of the interaction between photons provided from the cocoon and cosmic rays accelerated in the jets. We find that IceCube-Gen2, a future neutrino telescope, with the second-generation gravitational wave detectors will probably be able to observe neutrino signals associated with gravitational waves with around 10 years of operation, regardless of the assumed value of the Lorentz factor of the jets. Neutrino observations may enable us to constrain the dissipation region of the jets. We apply this model to GRB 211211A, a peculiar long GRB whose origin may be a binary neutron-star merger. Our model predicts that IceCube is unlikely to detect any associated neutrino, but a few similar events will be able to put a meaningful constraint on the physical quantities of the prolonged engine activities.

Keywords: Neutrino astronomy (1100) — Particle astrophysics (96) — Gamma-ray bursts (629) — Gravitational wave astronomy(675) — Neutron stars (1108)

1. INTRODUCTION

Binary neutron star (BNS) mergers are one of the most important targets of gravitational-wave (GW) observations and electromagnetic (EM) follow-up observations. Immediately after the first BNS merger event, GW170817, a short gamma-ray burst (sGRB) was identified as an EM counterpart (Abbott et al. 2017a,b,c). Radio observations show the superluminal motion (Mooley et al. 2018a), and radio to X-ray counterparts are well modeled by off-axis afterglow emission from a structured relativistic jet (Mooley et al. 2018a,b; Troja et al. 2018; Ghirlanda et al. 2019; Lamb et al. 2019).

These studies support BNS mergers as the progenitor of sGRBs.

The formation mechanism and dissipation process of sGRB jets, however, are still unknown, despite a lot of theoretical and observational studies (Berger 2014). The standard afterglow scenario cannot explain typical X-ray lightcurves of sGRBs, where we see some excesses on a timescale of 10^2 - 10^5 seconds after the prompt emission (Norris & Bonnell 2006; Sakamoto et al. 2011; Kagawa et al. 2015, 2019; Kaneko et al. 2015). These emission components, called extended and plateau emissions, are considered evidence of prolonged central engine activity (Ioka et al. 2005; Perna et al. 2006; Metzger et al. 2008; Rowlinson et al. 2013; Gompertz et al. 2014; Kisaka & Ioka 2015; Kisaka et al. 2017). Current observations provide little constraint on the physical quantities of

late-time emission components, including composition, Lorentz factor, and dissipation radius.

High-energy neutrinos are considered a powerful probe to investigate the physical quantities of gamma-ray bursts (GRBs) (Waxman & Bahcall 1997; Guetta et al. 2004; Murase & Nagataki 2006a; Hümmer et al. 2012; Li 2012; He et al. 2012; Kimura et al. 2017). When jets dissipate their kinetic energy, electrons are non-thermally accelerated by some process, such as the first-order Fermi acceleration, and produce gamma-rays observed as GRBs. If protons of PeV to EeV energies are accelerated at the same time, photohadronic interactions can produce neutrinos with energies above PeV (Kimura 2022). Observing such neutrinos in addition to EM wave signals enables us to investigate the physical mechanism of GRBs.

The neutrino observatory, IceCube, has been detecting high-energy neutrinos from astrophysical objects and trying to determine their source for more than ten years (Aartsen et al. 2013, 2020; IceCube Collaboration et al. 2021). Despite the expectation of neutrino emission from GRBs, GRB analyses by IceCube Collaboration revealed no significant spatial and temporal associations between cosmic neutrino events and GRBs (Abbasi et al. 2010, 2011; Icecube Collaboration et al. 2012; Aartsen et al. 2015, 2016, 2017a; Abbasi et al. 2022a), which put an upper limit on neutrino emission from GRBs. Future cosmic high-energy neutrino detectors, such as IceCube-Gen2 (Aartsen et al. 2021), KM3Net/ARCA (Aiello et al. 2019), baikal-GVD (Avrorin et al. 2014), P-One (Agostini et al. 2020), and TRIDENT (Ye et al. 2022), will significantly increase the detection rate of cosmic neutrinos. We should estimate neutrino emissions from various environments to efficiently interpret the data.

When we consider prolonged engine activity, the matter ejected by the BNS merger can play an important role in the high-energy component of late-time emissions. BNS merger ejects outflowing material (ejecta), as confirmed by optical/infrared counterparts to GW170817 (Kasliwal et al. 2017; Kasen et al. 2017; Murguía-Berthier et al. 2017; Shibata et al. 2017; Tanaka et al. 2017). The sGRB jet can interact with the ejecta if the jet formation delay from the merger, which leads to the formation of a cocoon (Bromberg et al. 2011; Hamidani et al. 2020; Hamidani & Ioka 2021). The cocoon can provide photons into the dissipation region of prolonged jets. Leptonic emission considering the external photons from the cocoon has been discussed (Kimura et al. 2019; Toma et al. 2009), but hadronic emissions with the cocoon photons are not considered in detail.

In this study, we calculate the production of high-energy neutrinos through the interaction of photons with cosmic rays accelerated inside the jet, taking into account the cocoon photons entering the prolonged jet. We also calculate the possibility of detecting neutrinos at the late time of sGRBs associated with GWs, based on the sensitivities of IceCube and IceCube-Gen2 (IceCube Collaboration et al. 2021). The calculation shows that after ~ 10 years of observation by IceCube-Gen2, it is highly probable to observe one or more neutrinos in this scenario, or we can constrain the parameters with a 2 or 3 σ confidence level. This result is almost independent of the Lorentz factor of jets, which may enable us to put a stronger constraint on the dissipation radius than that without cocoon photons. We describe our model and show the neutrino spectra in Section 2. In Section 3, we discuss the probability of the neutrino detection with current and future detectors. In Section 4, we apply our model to GRB 211211A, a peculiar long GRB whose origin may be a BNS merger. Summary and discussion are described in Section 5. We use the notation $Q_X = Q/10^X$ in cgs unit unless otherwise noted and write Q' for the physical quantities in the comoving frame of the jet.

2. NEUTRINO PRODUCTION USING COCOON PHOTONS

2.1. Photon Distributions

Neutrinos from GRBs are mainly produced by photomeson production. We consider that cosmic-ray (CR) protons are accelerated at a dissipation region in the jets. Photon distributions in the dissipation region affect the resulting neutrino spectra. Here, we consider two photon components: non-thermal radiation inside the jets and thermal radiation from the cocoon.

We write the differential number density of the non-thermal component using Band function:

$$\frac{dn'^{\text{in}}}{d\varepsilon'_\gamma} = n_{\varepsilon'_\gamma, \text{nor}} \begin{cases} \varepsilon'^\alpha_\gamma \exp\left(-\frac{(2+\alpha)\varepsilon'_\gamma}{\varepsilon'_{\gamma, \text{pk}}}\right) & (\varepsilon'_\gamma \leq \chi \varepsilon'_{\gamma, \text{pk}}) \\ \varepsilon'^\beta_\gamma (\chi \varepsilon'_{\gamma, \text{pk}}/e)^{\alpha-\beta} & (\varepsilon'_\gamma > \chi \varepsilon'_{\gamma, \text{pk}}) \end{cases} \quad (1)$$

where α and β are the photon indices of X-rays below and above the peak, respectively, $\chi = (\alpha - \beta)/(2 + \alpha)$, $n_{\varepsilon'_\gamma, \text{nor}}$ is the normalization factor, and ε'_γ and $\varepsilon'_{\gamma, \text{pk}}$ are the photon energy and the spectral peak energy in the jet comoving frame, respectively. The normalization is determined so that $L_{X, \text{iso}} = 4\pi\Gamma_j^2 r_{\text{diss}}^2 c \int_{\varepsilon_{X, \text{min}}/\Gamma_j}^{\varepsilon_{X, \text{Max}}/\Gamma_j} d\varepsilon'_\gamma \varepsilon'_\gamma (dn'_\gamma/d\varepsilon'_\gamma)$ is satisfied, where $L_{X, \text{iso}}$ is the isotropic-equivalent luminosity in the X-ray band, r_{diss} is the dissipation radius, Γ_j is the Lorentz factor of the jets, and $\varepsilon_{X, \text{Max}}$, and $\varepsilon_{X, \text{min}}$ are the maximum and minimum energies of the X-ray band, respec-

tively. Observationally, the X-ray luminosity shows a correlation with the duration of the extended emission as (Kisaka et al. 2017)

$$L_{X,\text{iso}} = 2 \times 10^{49} \left(\frac{t_{\text{dur}}}{10^2 \text{ s}} \right)^{-2.5} \text{ erg s}^{-1}. \quad (2)$$

We give t_{dur} as a parameter, and use the $L_X - t_{\text{dur}}$ relation to estimate the photon number density and the jet power. The total photon luminosity is obtained by $L_{\gamma,\text{iso}} = 4\pi\Gamma_j^2 r_{\text{diss}}^2 c \int_{\varepsilon'_{\gamma,\text{min}}}^{\varepsilon'_{\gamma,\text{max}}} d\varepsilon'_\gamma \varepsilon'_\gamma (dn'_\gamma/d\varepsilon'_\gamma)$, where $\varepsilon'_{\gamma,\text{min}}$ and $\varepsilon'_{\gamma,\text{max}}$ are the minimum and maximum photon energies, respectively. We set $\varepsilon'_{\gamma,\text{min}} = 0.1 \text{ eV}$ and $\varepsilon'_{\gamma,\text{max}} = 10^6 \text{ eV}$ because the synchrotron self-absorption and the pair creation are effective below and above the energies, respectively (Murase & Nagataki 2006b). The values of $\varepsilon'_{\gamma,\text{min}}$ and $\varepsilon'_{\gamma,\text{max}}$ do not strongly affect the results of this paper.

We use one-zone approximation for the cocoon as discussed in Kimura et al. (2019). The cocoon temperature is obtained as $T_{\text{coc}} = [3\mathcal{E}_{\text{coc}}/(4\pi R_{\text{coc}}^3 a_{\text{rad}})]^{1/4}$, where a_{rad} , $R_{\text{coc}} = 3.0 \times 10^{12} t_{\text{dur},2.5} \text{ cm}$, and \mathcal{E}_{coc} are the radiation constant, the cocoon radius, and the thermal energy of the cocoon, respectively. \mathcal{E}_{coc} is obtained by $\mathcal{E}_{\text{coc}} = \mathcal{E}_{\text{adi}} + \mathcal{E}_{\text{rad}}$, where $\mathcal{E}_{\text{adi}} = 8.8 \times 10^{44} t_{\text{dur},2.5}^{-1} \text{ erg}$ and $\mathcal{E}_{\text{rad}} = 9.3 \times 10^{44} t_{\text{dur},2.5}^{-0.3} \text{ erg}$ represent the contributions by the initial thermal energy of ejecta and by the radioactive decay of neutron-rich nuclei in the ejecta.

The photons in the cocoon need to diffuse into the jet to work as an external photon field. Taking this effect into account, the spectrum of the thermal external photons entering into the dissipation region from the cocoon is given by

$$\varepsilon'_\gamma \frac{dn'^{\text{ex}}}{d\varepsilon'_\gamma} = \Gamma_j \frac{8\pi(\varepsilon'_\gamma/\Gamma_j)^3}{h^3 c^3} \frac{1}{\exp[\varepsilon'_\gamma/(\Gamma_j k_B T_{\text{coc}})] - 1} \times e^{-\tau}, \quad (3)$$

where T_{coc} is the cocoon temperature, τ is the lateral optical depth of the jet, respectively, h is the Planck constant, k_B is the Boltzmann constant, and c is the speed of light. Hereafter, we call this component cocoon photons. The lateral optical depth is estimated to be $\tau = L_{k,\text{iso}} \sigma_T \theta_j / (4\pi r_{\text{diss}} \Gamma_j^2 m_p c^3) = 3.2 L_{k,\text{iso},50.5} r_{\text{dis},12}^{-1} \Gamma_{j,2}^{-2} (\theta_j/5^\circ)$, where σ_T , θ_j , and $L_{k,\text{iso}}$ are Thomson cross-section, opening angle of the jet and isotropic-equivalent kinetic luminosity, respectively. $L_{k,\text{iso}}$ is estimated to be $L_{k,\text{iso}} = L_{p,\text{iso}}/\epsilon_p = \xi_p L_{\gamma,\text{iso}}/\epsilon_p = 30 (\xi_p/10)(\epsilon_p/0.33)^{-1} L_{\gamma,\text{iso}}$, where $L_{p,\text{iso}}$ is the luminosity of accelerated protons, and ξ_p and ϵ_p are parameters.

We ignore the cocoon photons for $R_{\text{coc}} < r_{\text{diss}}$ because the cocoon does not cover the dissipation region for such a condition. This is a rough approximation because the

number of cocoon photons provided in the dissipation region should change smoothly, but it does not significantly affect the results because $R_{\text{coc}} > r_{\text{diss}}$ is satisfied in most cases in this study.

Recently, Hamidani & Ioka (2022) showed that a large fraction of cocoon is confined in the ejecta. If we apply the simulation to our model, \mathcal{E}_{coc} can be 200 times lower, and the temperature and number density of the cocoon photons can decrease by a factor of $(1/100)^{1/4}$ and $(1/100)^{3/4}$, respectively. However, this effect does not change the results dramatically because the protons lose all the energies owing to a high cocoon photon density even for such a low temperature (see Eq.A5).

2.2. Neutrino Spectra

Particle acceleration processes occurring in astrophysical environments usually lead to a power-law distribution function (e.g., Blandford & Eichler 1987; Guo et al. 2020), and we represent the cosmic-ray (CR) distribution function in the engine-rest frame as

$$\frac{dN_p}{d\varepsilon_p} = N_{\varepsilon_p,\text{nor}} \left(\frac{\varepsilon_p}{\varepsilon_{p,\text{cut}}} \right)^{-p_{\text{inj}}} \exp\left(-\frac{\varepsilon_p}{\varepsilon_{p,\text{cut}}}\right), \quad (4)$$

where $\varepsilon_{p,\text{cut}}$ is the proton cutoff energy and $N_{\varepsilon_p,\text{nor}}$ is the normalization factor. $N_{\varepsilon_p,\text{nor}}$ is determined by $L_{p,\text{iso}} t_{\text{dur}} = \xi_p L_{\gamma,\text{iso}} t_{\text{dur}} = \int_{\varepsilon_{\text{min}}}^{\infty} d\varepsilon_p \varepsilon_p (dN_p/d\varepsilon_p)$. The cutoff energy is determined by the balance between acceleration and cooling timescales. We use $\varepsilon_{p,\text{min}} = \Gamma_j \varepsilon'_{\text{min}} = 3\Gamma_j m_p c^2$ as the minimum energy of cosmic-ray protons, and ξ_p is the cosmic-ray loading parameter (Murase & Nagataki 2006a).

The acceleration timescale is estimated to be $t'_{\text{acc}} = \varepsilon'_p/(ceB')$, where $B' = \sqrt{2L_{\gamma,\text{iso}}\xi_B/(c\Gamma_j^2 r_{\text{diss}}^2)}$ is magnetic field in the comoving frame.

The cooling rate is given by $t'_{\text{cool}} = t'_{\text{ad}} + t'_{\text{BH}} + t'_{p\gamma} + t'_{\text{syn}}$, where each term represents adiabatic cooling, Bethe-Heitler process, photomeson production, and synchrotron cooling, respectively. The adiabatic and the synchrotron cooling timescales are given by $t'_{\text{ad}} = r_{\text{diss}}/(\Gamma_j c)$ and $t'_{\text{syn}} = 6\pi m_p^4 c^3/(m_e^2 \sigma_T B'^2)$, respectively. The cooling rates for Bethe-Heitler and photomeson production processes are estimated to be

$$t'_{p\gamma/\text{BH}} = \frac{c}{2\gamma_p'^2} \int_{\bar{\varepsilon}_{\text{th}}}^{\infty} d\bar{\varepsilon}_\gamma \sigma(\bar{\varepsilon}_\gamma) \kappa(\bar{\varepsilon}_\gamma) \bar{\varepsilon}_\gamma \int_{\bar{\varepsilon}_\gamma/2\gamma_p}^{\infty} d\varepsilon'_\gamma \varepsilon'^{\prime-2} \frac{dn'_\gamma}{d\varepsilon'_\gamma}, \quad (5)$$

where $\gamma'_p = \varepsilon'_p/(m_p c^2)$ is the Lorentz factor of protons and $\bar{\varepsilon}_{\text{th}}$, $\sigma(\bar{\varepsilon}_\gamma)$ and $\kappa(\bar{\varepsilon}_\gamma)$ are the threshold energy, the cross-section, and inelasticity for each reaction in the proton rest frame, respectively. We use the fitting formulae based on GEANT4 for the cross-section and inelasticity for photomeson production (Murase &

Nagataki 2006a) and analytic fitting formulae given in Stepney & Guilbert (1983); Chodorowski et al. (1992) for Bethe-Heitler process. We define $t_{p\gamma,\text{int}}$, $t_{\text{BH,int}}$, $t_{p\gamma,\text{int}}$, and $t_{\text{BH,coc}}$ as the cooling timescales using the internal photons and the cocoon photons, respectively.

The neutrino spectrum produced by the photomeson process and pion decay is approximately estimated to be

$$\frac{dN_{\nu_\mu}}{d\varepsilon_{\nu_\mu}} \approx \int d\varepsilon_\pi g(\varepsilon_\pi, \varepsilon_{\nu_\mu}) f_{\text{sup},\pi} \left(f_{p\gamma} \frac{dN_p}{d\varepsilon_p} \right) \Big|_{\varepsilon_p=5\varepsilon_\pi} \quad (6)$$

for muon neutrinos, and

$$\begin{aligned} \frac{dN_{\bar{\nu}_\mu}}{d\varepsilon_{\bar{\nu}_\mu}} &\approx \frac{dN_{\nu_e}}{d\varepsilon_{\nu_e}} \\ &\approx \int d\varepsilon_\mu g(\varepsilon_\mu, \varepsilon_{\nu_e}) f_{\text{sup},\mu} \left(f_{\text{sup},\pi} f_{p\gamma} \frac{dN_p}{d\varepsilon_p} \right) \Big|_{\varepsilon_p=5\varepsilon_\mu=\frac{20}{3}\varepsilon_\mu} \end{aligned} \quad (7)$$

for anti-muon neutrinos and electron neutrinos, where $f_{p\gamma} = t'_{\text{cool}}/t'_{p\gamma}$, $f_{\text{sup},i}$, and $g(\varepsilon_i, \varepsilon_j)d\varepsilon_j$ are the pion production efficiency by photomeson production, the suppression factor by the pion and muon coolings, and the distribution function of the secondary particle j produced by the decay of the parent particle i of energy ε_i , respectively. The suppression factor is estimated to be $f_{\text{sup},i} = 1 - \exp(-t'_{i,\text{cool}}/t'_{i,\text{dec}})$, where $t'_{i,\text{dec}}$ and $t'_{i,\text{cool}}$ are the lifetime and the cooling timescale of each particle in the comoving frame of the jet, respectively. The lifetime is given by $t'_{i,\text{dec}} = t_i \varepsilon'_i / (m_i c^2)$, where t_i is the lifetime in the particle rest frame, and m_i is the mass of a particle. $t'_{i,\text{cool}}$ is estimated to be $t'_{i,\text{cool}}^{-1} = t'_{i,\text{syn}}^{-1} + t'_{\text{ad}}^{-1}$, where $t'_{i,\text{syn}} = 6\pi m_i^4 c^3 / m_e^2 \sigma_T B^2 \varepsilon'_i$. Here, we assume that all pions produced by the photomeson production with ε_p have $\varepsilon_\pi = 0.2\varepsilon_p$, and all muon produced by the decay of pions with ε_π have $\varepsilon_\mu = (3/4)\varepsilon_\pi$. We approximate $g(\varepsilon_\pi, \varepsilon_{\nu_\mu}) = 4\Theta(\varepsilon_\pi - 4\varepsilon_{\nu_\mu})/\varepsilon_\pi$ and $g(\varepsilon_\mu, \varepsilon_{\nu_e}) = 3\Theta(\varepsilon_\mu - 3\varepsilon_{\nu_e})/\varepsilon_\mu$, where $\Theta(x)$ is Heaviside step function, because they imitate energy distributions for the two-body decay. This treatment can approximately account for the low-energy tail of the neutrino spectrum, which would affect the detectability of neutrinos.

Taking account of the neutrino mixing, we can approximately obtain the neutrino fluences measured at the Earth as (e.g., Becker 2008)

$$\phi_{\nu_e+\bar{\nu}_e} \approx \frac{10}{18}\phi_{\nu_e+\bar{\nu}_e}^0 + \frac{4}{18}(\phi_{\nu_\mu+\bar{\nu}_\mu}^0 + \phi_{\nu_\tau+\bar{\nu}_\tau}^0) \quad (8)$$

$$\phi_{\nu_\mu+\bar{\nu}_\mu} \approx \frac{4}{18}\phi_{\nu_e+\bar{\nu}_e}^0 + \frac{7}{18}(\phi_{\nu_\mu+\bar{\nu}_\mu}^0 + \phi_{\nu_\tau+\bar{\nu}_\tau}^0), \quad (9)$$

where $\phi_i^0 = (dN_i/d\varepsilon_i)/(4\pi d_L^2)$ is the neutrino fluence measured on the Earth assuming that the flavor ratio is fixed at the source, and d_L is the luminosity distance.

Figure 1 shows the acceleration and cooling timescales of protons as a function of energy (see Table 1 for our fiducial parameter set for extended and plateau emission). For our extended emission models, the photomeson production is the most efficient cooling process for $\varepsilon'_p \gtrsim 10 - 100$ TeV whereas the adiabatic loss is the most efficient for $\varepsilon'_p \lesssim 10 - 100$ TeV. The Bethe-Heitler process is not effective for any parameters due to its relatively low effective cross-section. The synchrotron cooling is also not effective because of the heavy mass of a proton and the moderate magnetic field. For the plateau emission models, the adiabatic loss is the most efficient except for $\varepsilon'_p \gtrsim 10$ PeV for $\Gamma_j = 10$. This is because their lower cocoon photon density.

The fluences of $\nu_\mu + \bar{\nu}_\mu$ for the fiducial parameters and for some other parameters are shown in Figure 2. In Appendix A, we show analytic expression of the fluence for the extended emission model with fiducial parameters (blue lines), which is dominated by cocoon photons. We also show the parameter dependence there.

For the cases with the other parameter sets shown in the panels (a) and (b) in Figure 2, the neutrinos are mainly produced by interaction with the internal photons. For $\Gamma_j = 20$, $t_{\text{dur}} = 10^{2.5}$, $\tau \sim 100$ is achieved, and the cocoon photons cannot diffuse into the dissipation region in such a high optical depth. For $\Gamma_j = 200$, $t_{\text{dur}} = 10^{1.5}$ s, $R_{\text{coc}} < r_{\text{diss}}$ is satisfied, and the cocoon photons cannot contribute to the neutrino emission. The neutrino spectra dominated by internal photons are roughly expressed by broken power law shapes with exponential cutoff that reflects spectra of internal photons and protons.

The parameter dependence of these neutrino spectra is consistent with previous studies that consider only internal photons (Waxman & Bahcall 1998; Zhang & Kumar 2013; Kimura et al. 2017; Kimura 2022). The neutrino spectra exhibit two break points: the low-energy break due to the photon spectral break and the high-energy break due to the pion cooling. The relativistic beaming effect leads to $t_{\text{ad}}^{-1} \propto \Gamma_j$ and $t_{p\gamma,\text{int}}^{-1} \propto \Gamma_j^{-1}$, which can be seen in Figure 1 by comparing the top-left and top-middle panels. In this case, the neutrino fluence is written as $\phi_{\nu_\mu} \propto t_{p\gamma,\text{int}}^{-1}/t_{\text{ad}}^{-1} \propto \Gamma_j^{-2}$. We can see this dependence by comparing the peaks by internal photons for $\Gamma_j = 20$ (orange dashed line) and for $\Gamma_j = 200$ (blue thin dashdot line) in panel (a) of Figure 2. For the case with $\Gamma_j = 200$ and $t_{\text{dur}} = 10^{1.5}$ s, $t_{p\gamma}^{-1}$ and the fluence of neutrino is much higher than those for other parameters, because we set the luminosity $10^{2.5}$ times higher than that for fiducial parameters based on Eq. (2).

Neutrino fluences from plateau emissions are much lower than those for extended emissions. The difference

Table 1. fiducial parameters

Parameters	Γ_j	t_{dur} (s)	$L_{X,\text{iso}}$ (erg/s)	r_{diss} (cm)	$\varepsilon_{\gamma,\text{pk}}$ (keV)		
Extended	200	$10^{2.5}$	10^{48}	10^{12}	10		
Plateau	100	10^4	10^{46}	10^{13}	1		
Shared	α	β	p_{inj}	ξ_p	ξ_B	$\varepsilon_{X,\text{min}}, \varepsilon_{X,\text{max}}$ (keV)	d_L (Mpc)
	-0.5	-2	2.0	10	0.33	0.3, 10 (XRT)	300

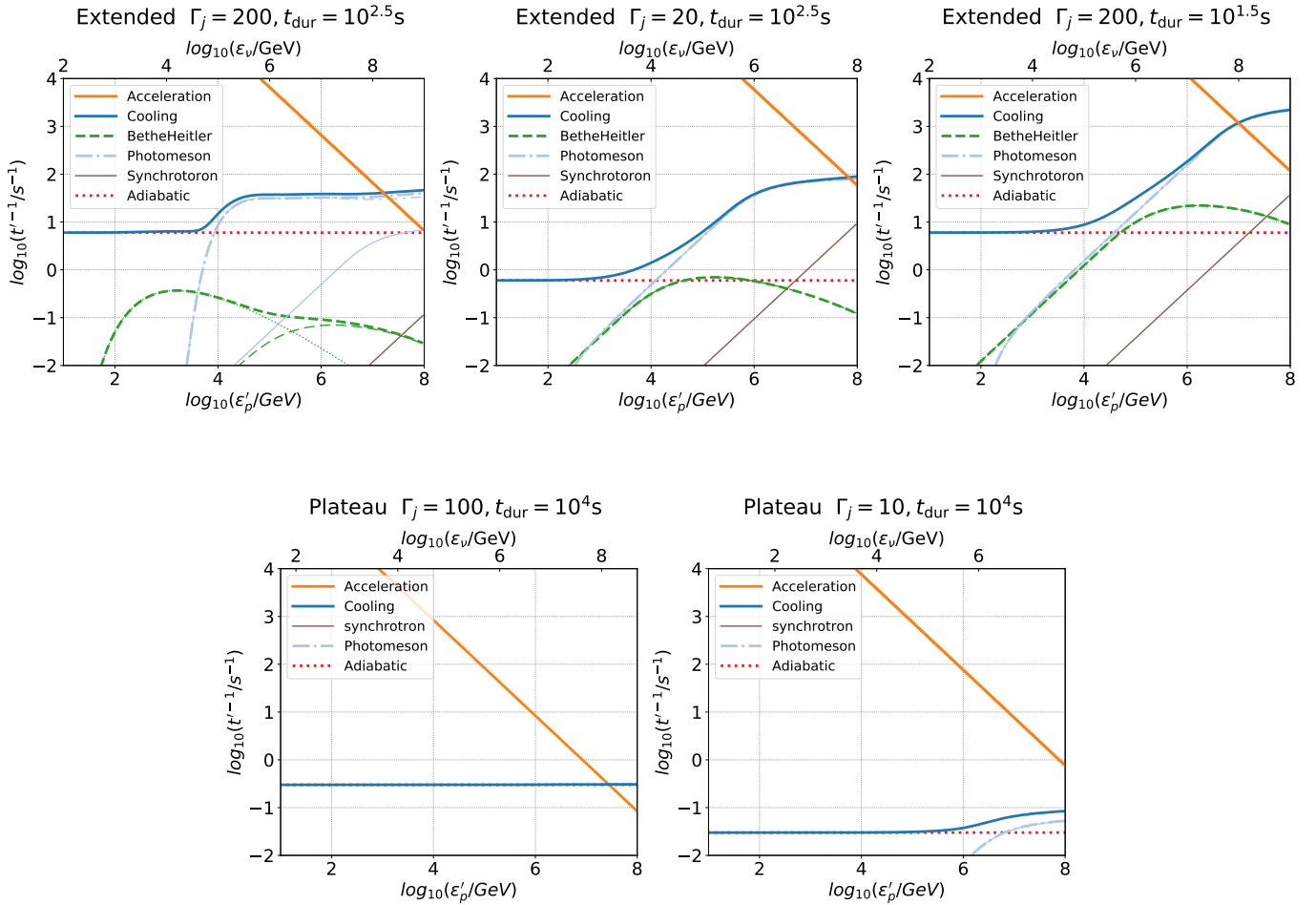


Figure 1. Acceleration and cooling rates for protons at the dissipation region in the comoving frame of the jet with various parameter sets. The thick orange lines and thick blue lines represent the acceleration timescales and total cooling timescales, respectively. The red thick-dotted, the lightblue-thick-dot-dashed, and the green-thick-dashed lines represent $t_{\text{ad}}'^{-1}$, $t_{p\gamma}'^{-1}$, and $t_{\text{BH}}'^{-1}$, respectively. The lightblue-thin-solid and the lightblue-thin-dot-dashed lines represent $t_{p\gamma,\text{int}}'^{-1}$ and $t_{p\gamma,\text{coc}}'^{-1}$, respectively. The green-thin-dashed and the green-thin-dotted lines represent $t_{\text{BH,int}}'^{-1}$ and $t_{\text{BH,coc}}'^{-1}$, respectively.

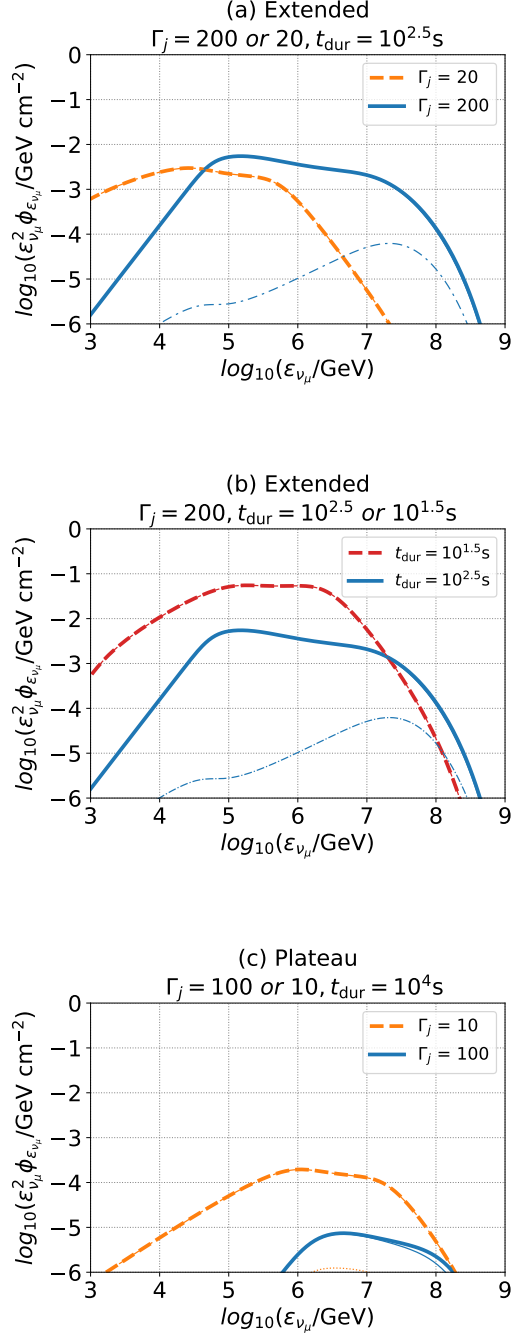


Figure 2. Neutrino fluences at the Earth. The thick lines are the total fluence and the thin lines are the contributions by the internal photons (in panels (a) and (b)) or cocoon photons (panel (c)). (a) Neutrino spectra for the extended emission models. The blue lines are for our fiducial parameter set, while the orange lines are for $\Gamma_j = 20$. The blue-thin-dot-dashed line is the contribution by the internal photons. (b) Neutrino spectra for extended emission model. The blue lines are the same as (a). The red lines are for $t_{\text{dur}} = 10^{1.5} \text{ s}$. (c) Neutrino spectra for plateau emission models. The blue lines are for our fiducial parameters, while the orange line is for $\Gamma_j = 10$.

between extended and plateau emissions is caused by the difference in the luminosity and the duration of the jet (see Table 1 for difference between extended and plateau emission). For the plateau emission, the total energy of injected protons, $L_{\gamma, \text{iso}} t_{\text{dur}}$ are almost the same as that for extended emission. On the other hand, photon number density for plateau emission is much less than that for extended emission because the longer duration leads to a low temperature cocoon due to the expansion. This results in a low cocoon photon number density at the dissipation region, causing a lower neutrino production rate for plateau emissions.

3. DETECTION PROSPECTS

We discuss prospects for neutrino detection associated with gravitational waves. Neutrino spectra from the extended emissions have a peak of $\sim 5.4 \times 10^{-3} \text{ GeV cm}^{-2}$ at $\epsilon_{\nu} \sim \text{PeV}$, which is comparable to the design sensitivity for a transient object for IceCube-Gen2 (Aartsen et al. 2021). These neutrinos should be detectable if we stack multiple sGRBs with extended emission, which requires long-term operation. Since neutrinos from plateau emissions are too weak to be detected by near-future experiments, the following discussion focuses on the detectability of neutrinos from extended emissions.

3.1. Neutrino Detection from a sGRB

The expected number of ν_{μ} -induced events is estimated to be

$$\bar{N}_{\nu_{\mu}} = \int d\epsilon_{\nu_{\mu}} \phi_{\nu_{\mu} + \bar{\nu}_{\mu}}(\epsilon_{\nu_{\mu}}) A_{\text{eff}}(\delta, \epsilon_{\nu_{\mu}}), \quad (10)$$

where A_{eff} is effective area for a detector and δ is declination angle. We use A_{eff} given in the 10-year point-source analysis (IceCube Collaboration et al. 2021), because this has a finer grid in δ than that used in the GRB analyses (Aartsen et al. 2017a). We assume that the effective area of IceCube-Gen2 is 5 times larger than that of IceCube.

We estimate $\bar{N}_{\nu_{\mu}}$ for various values of Γ_j and δ , whose results are shown in Figure 3. We use the fiducial parameters for other parameters, including $d_L = 300 \text{ Mpc}$, as shown in Table 1. The gray dashed line represents the expected number averaged over the solid angle without the cocoon photons. This line is proportional to Γ_j^{-2} for $\Gamma_j < 100$ due to Lorentz beaming effect, and to Γ_j^{-4} for $\Gamma_j > 100$ additionally because the low-energy break is higher than the energy range where IceCube is sensitive. The black solid line represents the expected number averaged over the solid angle with the cocoon photons. This line is overlapped with that without the cocoon

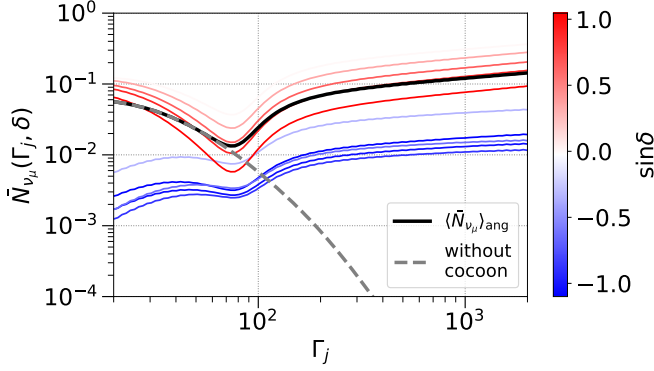


Figure 3. The expected number of ν_μ -induced events as a function of Γ_j (colored-thin lines). The color bar represents the declination angle. The black-solid line represents the expected number averaged over the solid angle. The gray-dashed line represents the expected number averaged over the solid angle without the cocoon photons.

photons for $\Gamma_j < 100$, since cocoon photons are negligible due to the shielding caused by large values of τ . For $\Gamma_j > 100$, the two lines separate from each other, due to the contribution of the cocoon photons. We find that if we take the cocoon photons into account, \bar{N}_{ν_μ} has a relatively weak dependence on Γ_j , because the neutrino peak fluence does not strongly depend on Γ_j when the cocoon photons are dominant, as shown in Appendix A. The expected number is slightly higher for a higher Γ_j as the muon and pion coolings are inefficient for a higher Γ_j .

The dependence on the declination angle is caused by the effective area of IceCube. IceCube efficiently detects neutrinos from the equatorial plane. In the southern hemisphere, the low-energy neutrinos cannot be detected due to the atmospheric muons. In the northern hemisphere, the high-energy neutrinos are absorbed by the Earth, which reduces the neutrino detection rate. For low Γ_j , the main component is internal photons and the peak of neutrino fluence is lower than PeV, where the atmospheric background is stronger. Thus, the value of \bar{N}_{ν_μ} is lower for a lower Γ_j in the Southern sky although the peak fluence is higher as $\phi_{\nu_\mu} \propto \Gamma_j^{-2}$. The probability of detecting more than one neutrino is given by

$$p_{n \geq 1}(\delta) = 1 - \exp(-\bar{N}_{\nu_\mu}). \quad (11)$$

This probability depends on δ , and we calculate the probability averaged over the solid angle by ¹

$$\langle p_{n \geq 1} \rangle_{\text{ang}} = \frac{1}{4\pi} \int d\Omega p_{n \geq 1}(\delta). \quad (12)$$

¹ The probability differs from $p_{n \geq 1}(\langle \bar{N}_{\nu_\mu} \rangle_{\text{ang}}) = 1 - \exp[-\int d\Omega \bar{N}_{\nu_\mu} / (4\pi)]$.

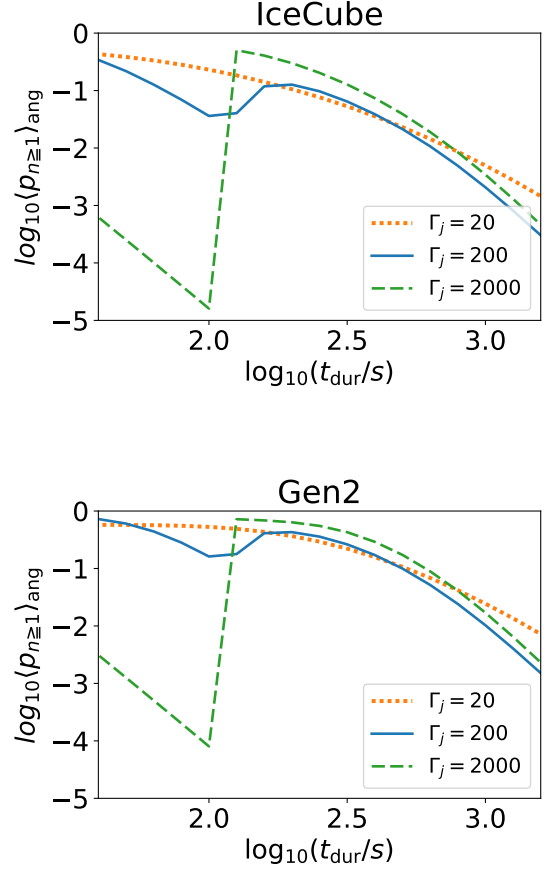


Figure 4. The probability of detecting more than 1 neutrinos as a function of t_{dur} . The upper and lower panel are the models for IceCube and IceCube-Gen2, respectively. The dotted, solid, and dashed lines represent the probability for $\Gamma_j = 20, 200,$ and 2000 , respectively.

We calculate $\langle p_{n \geq 1} \rangle_{\text{ang}}$ for various t_{dur} by using Eq. (2), and find that $\langle p_{n \geq 1} \rangle_{\text{ang}}$ highly depends on t_{dur} as shown in Figure 4. There is a jump at $t_{\text{dur}} = 10^2$ s for $\Gamma_j = 2000$, caused by the condition of no cocoon photons, $R_{\text{coc}} = \beta_{\text{coc}} c t_{\text{dur}} < r_{\text{diss}}$. The jump is an artifact because the number density of the cocoon photons in the dissipation region should change more smoothly. The bump at $t_{\text{dur}} \sim 200$ s for $\Gamma_j = 200$ is caused by the shielding of cocoon photons due to the high optical depth. For $t_{\text{dur}} > 100$ s, the expansion of the cocoon decreases the cocoon temperature and the photon number density, leading to a low neutrino fluence for a high value of t_{dur} . For $t_{\text{dur}} < 100$ s, the internal photons dominate because $r_{\text{diss}} > R_{\text{coc}}$ is satisfied, and $\langle p_{n \geq 1} \rangle_{\text{ang}}$ is high for a low value of t_{dur} due to $L_{X,\text{iso}} \propto (t_{\text{dur}}/10^2 \text{ s})^{-2.5}$.

3.2. Prospects for detecting neutrinos associated with GWs

We estimate the expected number of neutrino detection associated with GWs, taking into account the distribution of t_{dur} and $L_{X,\text{iso}}$. We assume that the distribution of t_{dur} is lognormal:

$$F(t_{\text{dur}}) = \frac{dN_{t_{\text{dur}}}}{d\log_{10}(t_{\text{dur}})} = F_0 \exp\left(-\frac{(\log_{10}(t_{\text{dur}}/t_{\text{dur},0}))^2}{2\sigma_{\log_{10}t_{\text{dur}}}^2}\right), \quad (13)$$

where $t_{\text{dur},0}$ and $\sigma_{\log_{10}t_{\text{dur}}}^2$ are the mean and variance of the duration, respectively. We fit the data of extended emission listed in [Kisaka et al. \(2017\)](#) to obtain the values of $t_{\text{dur},0} = 10^{2.4}$ s and $\sigma_{\log_{10}t_{\text{dur}}}^2 = 8.3 \times 10^{-2}$.

The probability of detecting neutrinos from a sGRB is given by

$$P_{n \geq 1} = \int d(\log_{10} t_{\text{dur}}) F(t_{\text{dur}}) \langle p_{n \geq 1} \rangle_{\text{ang}}. \quad (14)$$

We show dependence of $P_{n \geq 1}$ on d_L in Figure 5. The behavior of the line for each Γ_j is roughly the same for each d_L . $P_{n \geq 1} \propto d_L^{-2}$ for high d_L is consistent with $\phi_{\nu_\mu} \propto d_L^{-2}$ for a fixed luminosity. Assuming the uniform distributions of the location and timing of sGRBs, we can estimate the probability of detecting more than one neutrino associated with GW signal in T_{op} (yr) to be

$$q(T_{\text{op}}) = 1 - \exp\left(-T_{\text{op}} R_{\text{sGRB}} 4\pi \int^{300\text{Mpc}} d(d_L) d_L^2 P_{n \geq 1}\right), \quad (15)$$

where $R_{\text{sGRB}} = 8 \text{ Gpc}^{-3} \text{ yr}^{-1}$ is the event rate of sGRB (e.g., [Coward et al. 2012](#)).

The relation between q and T_{op} for IceCube (the thick lines) and for IceCube-Gen2 (the thin lines) are shown in Figure 6. We can constrain our fiducial parameter set for 2σ (3σ) confidence level within ~ 10 (~ 15) years of operation by IceCube-Gen2, although it would take more than 25 years by IceCube even for the most optimistic case. This indicates the importance of IceCube-Gen2 for detecting neutrinos from sGRBs and revealing the characteristics of prolonged jets.

We set the maximum luminosity distance as 300 Mpc, taking into account the sensitivity limit of BNS mergers for the second-generation GW detectors. Then, R_{sGRB} should be the rate of local sGRB though it has large uncertainty due to the low number of the local sGRBs ([Wanderman & Piran 2015](#); [Rouco Escorial et al. 2022](#)). The bottom panel of Figure 6 shows that the result is sensitive to the rate, but the possibility becomes equivalent to 2σ within 20 years of operation. We need to determine the local sGRB rate to make a more solid prediction for neutrino detection. In 20 years, the development of GW observatories will enable us to observe BNS mergers far from more than 300Mpc. This will dramatically increase the GW events, which possibly leads

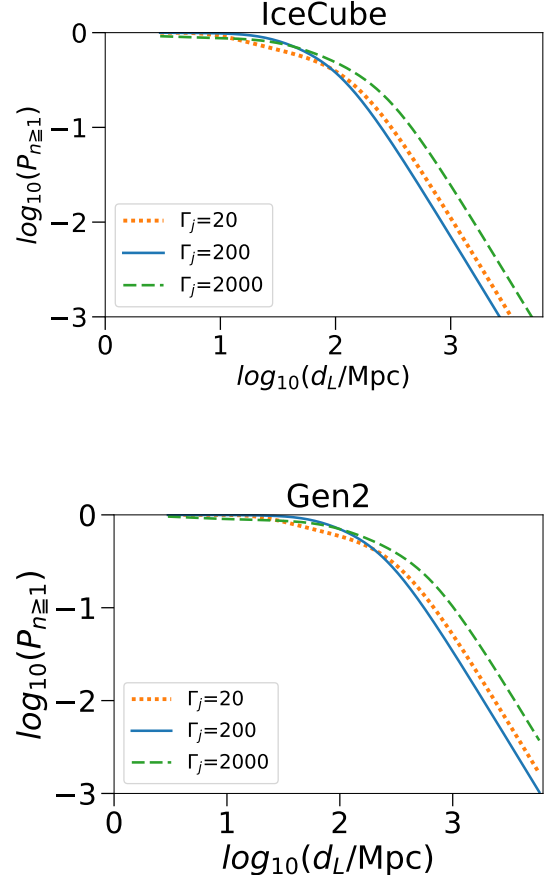


Figure 5. The probability of detecting more than one neutrinos as a function of d_L . The upper and lower panel are models for IceCube and IceCube-Gen2, respectively. The dotted, solid, and dashed lines represent probability for $\Gamma_j = 20$, 200, and 2000, respectively.

to an earlier detection of a neutrino associated with a GW event.

4. GRB 211211A

GRB 211211A is a long GRB whose prompt emission lasts for 13 s, followed by a soft extended component with a duration of 55 s ([Yang et al. 2022](#)). The progenitor of the GRB is, however, thought to be a merger of compact objects. Its host galaxy candidate is located at $d_L \simeq 350$ Mpc, and the GRB occurred at the outskirts of the galaxy. The prompt burst exhibits typical observational features of sGRBs, such as the negligible temporal lag, short variability timescale, and the position of the $\varepsilon_{\gamma,\text{pk}} - E_{\text{iso}}$ relation ([Troja et al. 2022](#)). The tentative evidence of kilonova associated with the GRB also supports the BNS merger origin ([Rastinejad et al. 2022](#)).

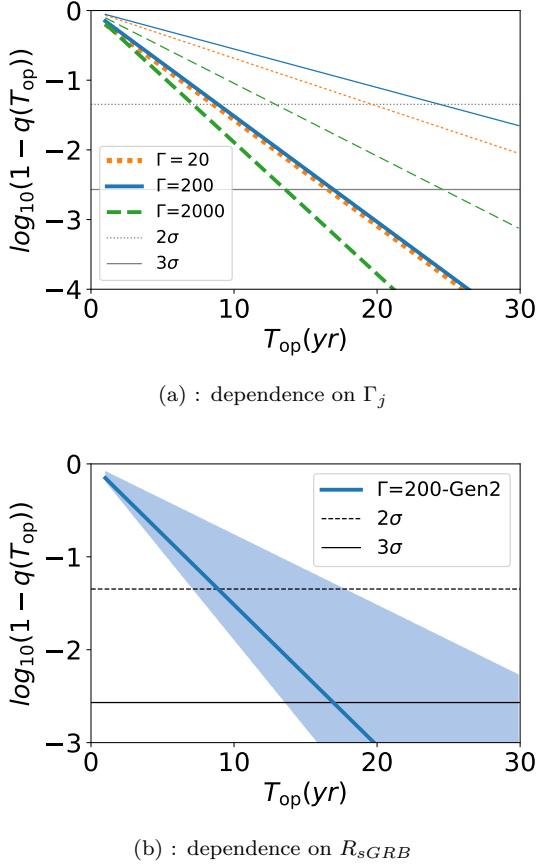


Figure 6. The probability of neutrino detection against the operation time. The thin horizontal lines correspond to the significance of 2σ and 3σ . (a) Thick and thin lines represent the models for IceCube and IceCube-Gen2, respectively. The dotted, solid, and dashed lines represent probability for $\Gamma_j = 20, 200,$ and $2000,$ respectively. (b) The uncertainty for the local sGRB rate. The colored region corresponds to the probability between the cases with $R_{sGRB} = 4 \text{ Gpc}^{-3} \text{ yr}^{-1}$ and with $R_{sGRB} = 10 \text{ Gpc}^{-3} \text{ yr}^{-1}$.

Additionally, GeV gamma-rays are observed with the GRB in $10^3 - 10^4$ s after the prompt emission (Mei et al. 2022). The gamma rays are explained by the external inverse Compton scattering process by non-thermal electrons accelerated in a prolonged jet (see Zhang et al. 2022 for another interpretation). Although the GeV signature is observed at a much later phase than the extended emission, the same system might be realized during the extended emission phase.

Neutrino associations with the GRB have not been reported by gamma-ray follow-up (GFU) search of IceCube. This implies that we can obtain an upper limit of neutrino flux from the GRB using the effective area of GFU (Aartsen et al. 2017b).

In Section 2.2, we show that neutrino emission with plateau emission is not detectable by IceCube and

IceCube-Gen2. This is consistent with the non-detection of neutrinos. On the other hand, it is expected that neutrinos could be found with extended emission because the luminosity of the extended emission is much higher than the plateau emission. To check the consistency of our model, we calculate $\bar{N}_{\nu\mu}$ from GRB 211211A based on our scenario.

The property of the event and its extended emission is summarized in Table 2 (see Table 1 of Yang et al. 2022 for other quantities). Since the duration of the extended emission is relatively short, the dissipation radius should be small, $r_{\text{diss}} \lesssim 5.3 \times 10^{11}$ cm, for the cocoon photons to enter into dissipation regions. The calculations are performed by setting $\Gamma = 10 - 5000$ and $r_{\text{diss}} = 10^{10} - 10^{13}$ cm though they include extreme parameters. The results are shown in Table 3 and Figure 7. These indicate that the expected numbers of neutrinos observed by IceCube are less than 1 for all the parameter sets. The expected number for GFU is also less than 1 because the effective area of GFU is smaller than that of the point source in the northern hemisphere ($\delta > 0$). These results are consistent with the absence of GFU alerts associated with GRB 211211A. We cannot constrain the parameter space with the current facilities.

The observation by IceCube-Gen2 is important. The circles in Figure 7 show parameters where the calculated expected numbers of neutrinos by IceCube are greater than 0.2. The effective area of IceCube-Gen2 is five times larger than that of IceCube, and IceCube-Gen2 will be able to detect a neutrino from GRB 211211A-like bursts for those parameters or put constraint on 68% confidence level.

The neutrino signals from GRB 211211A are stronger for low Γ_j region owing to the intense internal photon field. The neutrino signals can be stronger for a medium r_{diss} and high Γ_j region because of the cocoon photons. These results can be analytically understood by the following discussion.

First, we discuss the conditions when the internal photons are dominant. For efficient neutrino production, the pion production efficiency needs to be high. Considering the large effective area of IceCube around $\varepsilon_{\nu\mu} \sim 100$ TeV, the condition of efficient pion production is determined by $(t'_{\text{ad}}/t'_{p\gamma, \text{int}})|_{\varepsilon_{\nu\mu}=100 \text{ TeV}} \geq 1$. This condition can be represented by

$$r_{\text{dis},12} \leq 6.0 \Gamma_{j,2}^{-2} L_{\gamma, \text{iso},50} \left(\frac{\varepsilon_{\gamma, \text{pk}}}{100 \text{ keV}} \right)^{-1} \times \left[1 + 0.54 \left(\frac{\varepsilon_{\gamma, \text{pk}}}{100 \text{ keV}} \right) \Gamma_{j,2}^2 \right]^{-1}, \quad (16)$$

which is derived from Equation (28) in Kimura (2022). This condition is shown by red-solid line in Figure 7. In addition, the pion cooling needs to be inefficient.

Table 2. Properties of GRB 211211A

RA	Dec (= δ)		
14h 09m 05s	+27° 53' 01"		
t_{dur}	$\varepsilon_{\gamma,\text{pk}}$	α	β
(s)	(keV)		
55	82	-0.97	-2.02
Energy fluence	$L_{X,\text{iso}}$	$\varepsilon_{X,\text{min}}, \varepsilon_{X,\text{max}}$	d_L
(erg/cm ²)	(erg/s)	(keV)	(Mpc)
1.6×10^{-4}	4.3×10^{49}	15, 150 (BAT)	350

The condition of the inefficient pion cooling is determined by $\varepsilon_{\nu,\text{cool}} \geq 100$ TeV, where $\varepsilon_{\nu,\text{cool}}$ is defined by $(t'_{\pi,\text{cool}}|_{\varepsilon'_p=20\varepsilon_{\nu,\text{cool}}/\Gamma_j}/t'_{\pi,\text{dec}}|_{\varepsilon'_p=20\varepsilon_{\nu,\text{cool}}/\Gamma_j}) = 1$. The condition leads to

$$r_{\text{dis},12} \geq 4.6 \times 10^{-3} \Gamma_{j,2}^{-2} L_{\gamma,\text{iso},50}^{1/2} \left(\frac{\xi_B}{0.33} \right)^{1/2} + 2.5 \times 10^{-3}. \quad (17)$$

The first term of the right-hand-side is the contribution by the synchrotron cooling and the other is by the adiabatic cooling. The red-dotted line represents this condition.

Next, we consider the case where the cocoon photons are dominant. For efficient neutrino production, the cocoon needs to cover the dissipation region; $r_{\text{diss}} \leq R_{\text{coc}}$, which is shown as the blue-solid line. If this condition is satisfied, the cocoon photons always lead to the efficient neutrino production, i.e., $(t'_{\text{ad}}/t'_{p\gamma,\text{coc}})|_{\text{peak}} \geq 1$. The cocoon photons are shielded if the lateral optical depth, τ , is large. The strong shielding can be avoided if $e^{-\tau} \geq 1/10$ is satisfied. This condition can be rewritten as

$$r_{\text{dis},12} \geq 40 \times \Gamma_{j,2}^{-2} L_{\gamma,\text{iso},50} \times \ln 10. \quad (18)$$

This condition is shown in the blue-dashed line.

In summary, the neutrino production is efficient below the solid lines and above the dashed lines in Figure 7. In the red-colored region, the neutrinos are produced by the internal photons, whereas the cocoon photons are important in the blue-colored region.

5. SUMMARY AND DISCUSSION

We calculated the neutrino fluence emitted by the prolonged jet of sGRB, which can be associated with GW events. We take into account the photons entering into the jet from the cocoon formed by the jet-ejecta interaction. Owing to the contribution by the cocoon photons, the peak neutrino fluence has a weak dependence on the Lorentz factor of the jet, Γ_j . We found that the peak fluence is approximately 5.4×10^{-3} GeV cm⁻² at $\varepsilon_{\nu} \sim \text{PeV}$

Table 3. Expected neutrino number from GRB 211211A

$r_{\text{dis}}(\text{cm})$	Γ_j	20	200	2000
10^{13}		4.1×10^{-1}	5.3×10^{-3}	9.1×10^{-7}
10^{12}		3.0×10^{-1}	2.7×10^{-2}	6.0×10^{-6}
10^{11}		1.2×10^{-1}	7.5×10^{-2}	8.2×10^{-1}
10^{10}		2.1×10^{-2}	1.0×10^{-1}	1.1×10^{-4}

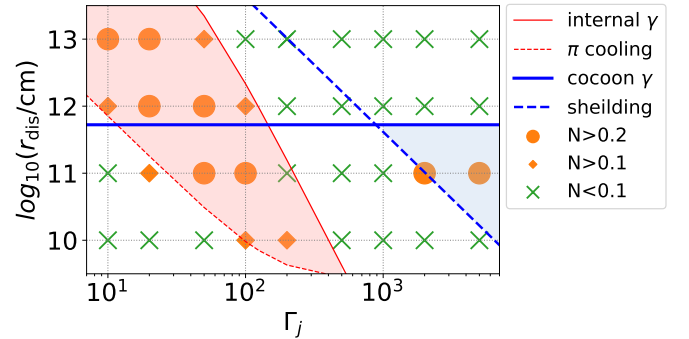


Figure 7. The chart of neutrino number from GRB 211211A. The orange circles, orange diamonds, the green crosses indicate the parameters for $0.2 < \bar{N}_{\nu\mu}$, $0.1 < \bar{N}_{\nu\mu} < 0.2$, and $\bar{N}_{\nu\mu} < 0.1$, respectively. The red-solid and blue-solid lines indicate the boundary for efficient pion production by internal and cocoon photons, respectively. The red-dashed line is the boundary for efficient pion cooling, and the blue-dashed line is the boundary for the shielding of the cocoon photons. Red-shaded and blue-shaded regions are parameter space where neutrinos are efficiently produced by internal and cocoon photons, respectively.

from a single sGRB with our fiducial parameters shown in Table 1. We expect that the expected number of the neutrino event will be 0.1 by IceCube, while it will be 0.5 by IceCube-Gen2. Assuming the homogeneous spatial distribution and the log-normal duration distribution of sGRBs, we found that the possibility of neutrino detection associated with GW events is sufficiently high if we continue to observe cosmic neutrinos with IceCube-Gen2 for 10 years. Even if the future observation results in no detection of neutrinos associated with GWs, we can put a strong constraint on the parameter space of the late-time jets. We also applied our model to GRB 211211A. We found that no associated neutrino signal in IceCube with GRB 211211A is consistent with our model, but we can put a meaningful constraint with future GRB 211211A-like events if IceCube-Gen2 is in operation.

We assumed that CRs are accelerated at the dissipation radius, but we need to be cautious about the condition for CR production. In the internal shock model, the

radiation mediated shock can be formed if the upstream of the shock is optically thick, which prevents CRs from being accelerated (Murase & Ioka 2013; Kimura et al. 2018). This effect can drastically reduce neutrino fluence. However, our scenario can avoid the condition even for $\Gamma_j = 20$ as long as the Lorentz factor of the shock upstream is as high as 100.

In addition, we should note that the energy density of the internal photon, $\int_{\varepsilon_{X,\min}/\Gamma_j}^{\varepsilon_{X,\max}/\Gamma_j} d\varepsilon'_\gamma \varepsilon'_\gamma (dn'_\gamma/d\varepsilon'_\gamma) = L_{X,\text{iso}}/(4\pi\Gamma_j^2 r_{\text{diss}}^2 c)$, can be modified if $\tau_j > 1$ is satisfied. The internal photon density can be constant in radius if a part of the kinetic energy of the jet dissipates inside the photosphere, as discussed in Rees & Mészáros (2005). In this case, our results are not affected. However, the photon luminosity at the dissipation region can be higher than that at the photosphere if the dissipation cannot compensate the energy loss by the adiabatic expansion. In this case, the internal photon density at the dissipation region is higher than that at the photosphere. Nevertheless, this effect has little influence on the neutrino fluence because of the efficient neutrino production, $f_{p\gamma} = 1$, for the cases with $\tau_j \gtrsim 1$. Therefore, our conclusions should be unchanged as long as CRs are accelerated at the given r_{diss} .

We can constrain other parameters, such as dissipation radius r_{diss} , more strongly than the previous study if we ignore the dependence on Γ_j . The case with $r_{\text{diss}} > 10^{12}$ cm will favor the internal shock model or Internal Collision-induced Magnetic Reconnection and Turbulence (ICMART; Zhang & Yan 2011; Zhang & Kumar 2013), while the case with $r_{\text{diss}} < 10^{12}$ cm would favor the dissipative photosphere scenario (Rees & Mészáros 2005).

The detection of neutrinos from the sGRBs will be a smoking-gun signature of the hadronic CR acceleration in the sGRB environment. This can constrain the composition of the jet in extended emission, i.e., whether the prolonged jets are leptonic or baryonic. Baryonic jets demand a baryon injection process into jets, such as neutron diffusion from neutron-rich matter (Beloborodov 2003; Levinson & Eichler 2003), which is thought to be the baryon injection process into the prompt jets. In the phase of the late-time emission, the mass accretion rate onto the remnant object might be too low to form a neutron-rich material (e.g., Kohri et al. 2005). Magnetar models are often discussed as a possible explanation of extended emissions only by the leptonic process (Dai & Lu 1998). Neutrino observations will potentially be able to rule out some leptonic models, which will clarify the jet launching mechanism.

Abbasi et al. (2022b) concludes that time-integrated fluences in 300 s after the event for all northern sGRBs

(183 events) are less than 1×10^{-1} GeV cm $^{-2}$ in total by analyzing the correlation of the GRB catalog detected by *Swift* or *Fermi* and IceCube data sets. This means that the upper limit of fluence from a single sGRB is about 5×10^{-4} GeV cm $^{-2}$ on average. The data include mostly the signals of sGRBs from cosmological distance, which is not the focus of our study. If we assume that the redshifts of the sGRBs analyzed in Abbasi et al. (2022b) are typically about $z \sim 0.5$ (corresponding to $d_L \sim 3$ Gpc), the upper limit of neutrino luminosity becomes about 3×10^{48} erg s $^{-1}$. The neutrino luminosity in our model, $\sim 5 \times 10^{47}$ erg s $^{-1}$, is lower than the upper limit and consistent with the IceCube data.

The high-energy gamma-ray observations also provide a test for our model. The astrophysical neutrinos are inevitably accompanied by gamma-rays produced by π^0 decay with the similar energy and luminosity, because the reaction rate of π^0 production is almost the same as that of π^\pm production. However, the peak energy of gamma-rays is not 100 TeV - PeV, because they are to cascade into lower energies by the interaction with low-energy photons. The resulting peak of the escaped photon spectrum is expected to be MeV - GeV. Gamma-rays in this energy band will be detected by future telescopes, such as eASTROGAM (De Angelis et al. 2017), GRAMS (Aramaki et al. 2020), and AMEGO-X (Caputo et al. 2022). The multi-messenger approach, using gamma-ray and the neutrino signals, will be a powerful tool to constrain the physical conditions of the dissipation region.

Neutrino detection associated with GWs enables us to probe the phenomena that cannot be investigated only by EM signals. Choked jet systems, where jets fail to break out from the stellar envelope or kilonova ejecta, are a good example (Murase & Ioka 2013; Kimura et al. 2018). The threshold timescale in the duration distribution of prompt emissions of sGRBs indicates the existence of such events (Moharana & Piran 2017). Matsumoto & Kimura (2018) showed that prolonged jet can break out from the ejecta even if prompt jet fails to penetrate it. In such a scenario, we cannot observe the emission from prompt jets but can observe the extended emission from the prolonged jets. X-ray observations found a few candidates for such a delayed breakout event (Xue et al. 2019), but it is difficult to confirm. Based on our model, we expect detection of neutrinos and GWs from the delayed breakout event. Thus, GW-neutrino association without prompt gamma rays would strongly support the scenario of the delayed breakout. The event rate of the choked jets is expected to be approximately 0.4 times lower than that of the successful sGRBs (Sarin et al. 2022), although it can be increased by the uncer-

tainty of the event rate of sGRBs and BNS mergers. If the fraction of the choked jet is on the high end, the delayed breakout will be a major component, and we will be able to detect much more GW-neutrino association. Thus, the GW-neutrino association can be a powerful tool to probe the central engine activity.

¹ This work is supported by Graduate Program on
² Physics for the Universe (GP-PU), Tohoku University
³ (R.M.), JSPS KAKENHI No. 22K14028 (S.S.K.) and
⁴ 18H01245 (K.T.). This work of K.M. is supported by
⁵ the NSF Grant No. AST-1908689, No. AST-2108466
⁶ and No. AST-2108467, and KAKENHI No. 20H01901.
⁷ S.S.K. acknowledges the support by the Tohoku Ini-
⁸ tiative for Fostering Global Researchers for Interdisci-
⁹ plinary Sciences (TI-FRIS) of MEXT's Strategic Profes-
¹⁰ sional Development Program for Young Researchers.

APPENDIX

A. ANALYTIC EXPLANATION OF NEUTRINO SPECTRA

In this section, we analytically estimate the neutrino fluence when the cocoon photons dominate over the internal photons. If we assume $g(\varepsilon_\pi, \varepsilon_{\nu_\mu}) = \delta(\varepsilon_\pi/4 - \varepsilon_{\nu_\mu})$ and $g(\varepsilon_\mu, \varepsilon_{\nu_e}) = \delta(\varepsilon_\mu/3 - \varepsilon_{\nu_e})$, the neutrino spectra are given by

$$\varepsilon_{\nu_\mu}^2 \frac{dN_{\nu_\mu}}{d\varepsilon_{\nu_\mu}} \approx \frac{1}{8} f_{p\gamma} f_{\text{sup},\pi} \varepsilon_p^2 \frac{dN_p}{d\varepsilon_p} \Big|_{\varepsilon_p=20\varepsilon_{\nu_\mu}} \quad (\text{A1})$$

$$\varepsilon_{\bar{\nu}_\mu}^2 \frac{dN_{\bar{\nu}_\mu}}{d\varepsilon_{\bar{\nu}_\mu}} \approx \varepsilon_{\nu_e}^2 \frac{dN_{\nu_e}}{d\varepsilon_{\nu_e}} \approx \frac{1}{8} f_{p\gamma} f_{\text{sup},\pi} f_{\text{sup},\mu} \varepsilon_p^2 \frac{dN_p}{d\varepsilon_p} \Big|_{\varepsilon_p=20\varepsilon_{\nu_\mu}}. \quad (\text{A2})$$

These are useful to understand the resulting spectrum analytically (e.g., [Kimura 2022](#), for a review). This expression assumes that all the decay products produced by a pion with ε_π share the same amount of energy: $\varepsilon_{\nu_\mu} \approx \varepsilon_{\nu_e} \approx \varepsilon_{\bar{\nu}_\mu} \approx \varepsilon_e \approx \varepsilon_\pi/4$.

To estimate $f_{p\gamma}$ and the fluence, we can roughly estimate $t'_{p\gamma}$ by using additional approximations. Considering only cocoon photons, which are the dominant component for the fiducial parameters, and $\sigma\kappa \sim \sigma_{0,\text{eff}}\theta(\bar{\varepsilon}_\gamma - \bar{\varepsilon}_{\text{th}})$ as an approximation, we can perform the calculation of Eq.(5). Using Eq.(69) of [Dermer et al. \(2012\)](#), we can obtain timescale of photomeson production with the cocoon photons as

$$\begin{aligned} t'_{p\gamma,\text{coc}}^{-1} &= \frac{16\pi k_B^3 T_{\text{coc}}^3 \sigma_{0,\text{eff}} \Gamma_j}{h^3 c^2} \int_{\bar{\varepsilon}'_p/\varepsilon'_p}^{\infty} dy y \ln(1 - e^{-y})^{-1} \\ &\sim \frac{16\pi k_B^3 T_{\text{coc}}^3 \sigma_{0,\text{eff}} \Gamma_j}{h^3 c^2} \begin{cases} \zeta(3) & (\varepsilon'_p \gg \bar{\varepsilon}'_p) \\ \bar{\varepsilon}'_p/\varepsilon'_p e^{-\bar{\varepsilon}'_p/\varepsilon'_p} & (\varepsilon'_p \ll \bar{\varepsilon}'_p), \end{cases} \end{aligned} \quad (\text{A3})$$

where $\bar{\varepsilon}'_p = (\bar{\varepsilon}_{\text{th}} m_p c^2)/(2k_B T_{\text{coc}} \Gamma_j)$ is the threshold energy of protons for photomeson production with typical cocoon photons, and $\zeta(x)$ is the zeta function. The lightblue-thin-dotted-dashed lines shown in [Figure 1](#), which is almost completely overlapped with the thick-dot-dashed line in our fiducial model, can be well explained by this approximate formula. $t'_{p\gamma,\text{coc}}^{-1}$ is constant for $\varepsilon'_p \gtrsim \bar{\varepsilon}'_p$, and it has an exponential cutoff at lower energies. The cutoff neutrino energy in the observer frame is estimated to be

$$\varepsilon_\nu \sim \frac{\bar{\varepsilon}'_p}{20\Gamma_j} = \frac{\bar{\varepsilon}_{\text{th}} m_p c^2}{40k_B T_{\text{coc}}} \sim 0.13 \left(\frac{\bar{\varepsilon}_{\text{th}}}{0.1 \text{ GeV}} \right) \left(\frac{k_B T_{\text{coc}}}{20 \text{ eV}} \right)^{-1} \text{ PeV} \quad (\text{A4})$$

which does not depend on Γ_j .

For $\varepsilon'_p > \tilde{\varepsilon}'_p$, we can write

$$t'^{-1}_{p\gamma,\text{coc}} \sim 88 \left(\frac{\sigma_{0,\text{eff}}}{6 \times 10^{-29} \text{ cm}^2} \right) \left(\frac{k_B T_{\text{coc}}}{20 \text{ eV}} \right)^3 \left(\frac{\Gamma_j}{200} \right) \text{ s}^{-1}. \quad (\text{A5})$$

Based on Figure 1, the photomeson production with the cocoon photons is the most efficient process, and all the protons of $\varepsilon'_p > \tilde{\varepsilon}'_p$ lose their energy. Thus, the peak fluence contributed by cocoon photons does not depend on Γ_j . Even for the case with $t'_{\text{ad}} < t'_{p\gamma,\text{coc}}$, both of the timescales have the same Γ_j dependence, and therefore, the pion production efficiency and the neutrino fluence do not depend on Γ_j as long as the cocoon photons are dominant for neutrino production.

The high-energy cutoff in the neutrino spectra is caused by the proton injection spectrum. The cutoff energy of protons in the observer frame depends on Γ_j . In the range, $t'_{\text{cool}} \sim t'^{-1}_{p\gamma,\text{coc}} \propto \Gamma_j$ is satisfied and t'^{-1}_{acc} is proportional to Γ_j^{-1} due to Lorentz transformation of magnetic field. This leads to $\varepsilon'_{p,\text{cut}} \propto \Gamma_j^{-2}$ and $\varepsilon_{p,\text{cut}} \propto \Gamma_j^{-1}$. The cutoff energy is $\varepsilon'_{p,\text{cut}} \sim 8.2 \times 10^6 (\Gamma_j/200)^{-2}$ GeV for the proton energy in the comoving frame of the jet and $\varepsilon_\nu \sim 8.2 \times 10^7 (\Gamma_j/200)^{-1}$ GeV for neutrino energy in the observer frame for the fiducial parameters.

For $\varepsilon_{\nu\mu} < 100$ TeV, the resultant fluence shown in Figure 2 is $\varepsilon_\nu^2 (dN_\nu/d\varepsilon_\nu) \propto \varepsilon_\nu^2$, while $f_{p\gamma,\text{coc}} \times \varepsilon_p^2 (dN_p/d\varepsilon_p)$ should have a cutoff feature. This is because of the different treatment of $g(\varepsilon_i, \varepsilon_j)$. The cutoff feature of the lower energy is not realistic since the decaying pions with the peak energy must produce neutrinos with energies lower than $(1/4)\varepsilon_\pi$.

REFERENCES

- Aartsen, M. G., Abbasi, R., Abdou, Y., et al. 2013, *PhRvL*, 111, 021103, doi: [10.1103/PhysRevLett.111.021103](https://doi.org/10.1103/PhysRevLett.111.021103)
- Aartsen, M. G., Ackermann, M., Adams, J., et al. 2015, *ApJL*, 805, L5, doi: [10.1088/2041-8205/805/1/L5](https://doi.org/10.1088/2041-8205/805/1/L5)
- Aartsen, M. G., Abraham, K., Ackermann, M., et al. 2016, *ApJ*, 824, 115, doi: [10.3847/0004-637X/824/2/115](https://doi.org/10.3847/0004-637X/824/2/115)
- Aartsen, M. G., Ackermann, M., Adams, J., et al. 2017a, *ApJ*, 843, 112, doi: [10.3847/1538-4357/aa7569](https://doi.org/10.3847/1538-4357/aa7569)
- . 2017b, *Astroparticle Physics*, 92, 30, doi: [10.1016/j.astropartphys.2017.05.002](https://doi.org/10.1016/j.astropartphys.2017.05.002)
- . 2020, *PhRvL*, 124, 051103, doi: [10.1103/PhysRevLett.124.051103](https://doi.org/10.1103/PhysRevLett.124.051103)
- Aartsen, M. G., Abbasi, R., Ackermann, M., et al. 2021, *Journal of Physics G Nuclear Physics*, 48, 060501, doi: [10.1088/1361-6471/abbd48](https://doi.org/10.1088/1361-6471/abbd48)
- Abbasi, R., Abdou, Y., Abu-Zayyad, T., et al. 2010, *ApJ*, 710, 346, doi: [10.1088/0004-637X/710/1/346](https://doi.org/10.1088/0004-637X/710/1/346)
- . 2011, *PhRvL*, 106, 141101, doi: [10.1103/PhysRevLett.106.141101](https://doi.org/10.1103/PhysRevLett.106.141101)
- Abbasi, R., Ackermann, M., Adams, J., et al. 2022a, arXiv e-prints, arXiv:2205.11410, <https://arxiv.org/abs/2205.11410>
- . 2022b, *ApJ*, 939, 116, doi: [10.3847/1538-4357/ac9785](https://doi.org/10.3847/1538-4357/ac9785)
- Abbott, B. P., Abbott, R., Abbott, T. D., et al. 2017a, *ApJL*, 848, L12, doi: [10.3847/2041-8213/aa91c9](https://doi.org/10.3847/2041-8213/aa91c9)
- . 2017b, *PhRvL*, 119, 161101, doi: [10.1103/PhysRevLett.119.161101](https://doi.org/10.1103/PhysRevLett.119.161101)
- . 2017c, *ApJL*, 848, L13, doi: [10.3847/2041-8213/aa920c](https://doi.org/10.3847/2041-8213/aa920c)
- Agostini, M., Böhmer, M., Bosma, J., et al. 2020, *Nature Astronomy*, 4, 913, doi: [10.1038/s41550-020-1182-4](https://doi.org/10.1038/s41550-020-1182-4)
- Aiello, S., Akrame, S. E., Ameli, F., et al. 2019, *Astroparticle Physics*, 111, 100, doi: [10.1016/j.astropartphys.2019.04.002](https://doi.org/10.1016/j.astropartphys.2019.04.002)
- Aramaki, T., Adrian, P. O. H., Karagiorgi, G., & Odaka, H. 2020, *Astroparticle Physics*, 114, 107, doi: [10.1016/j.astropartphys.2019.07.002](https://doi.org/10.1016/j.astropartphys.2019.07.002)
- Avrorin, A. D., Avrorin, A. V., Aynutdinov, V. M., et al. 2014, *Nuclear Instruments and Methods in Physics Research A*, 742, 82, doi: [10.1016/j.nima.2013.10.064](https://doi.org/10.1016/j.nima.2013.10.064)
- Becker, J. K. 2008, *PhR*, 458, 173, doi: [10.1016/j.physrep.2007.10.006](https://doi.org/10.1016/j.physrep.2007.10.006)
- Beloborodov, A. M. 2003, *ApJ*, 588, 931, doi: [10.1086/374217](https://doi.org/10.1086/374217)
- Berger, E. 2014, *ARA&A*, 52, 43, doi: [10.1146/annurev-astro-081913-035926](https://doi.org/10.1146/annurev-astro-081913-035926)
- Blandford, R., & Eichler, D. 1987, *PhR*, 154, 1, doi: [10.1016/0370-1573\(87\)90134-7](https://doi.org/10.1016/0370-1573(87)90134-7)
- Bromberg, O., Nakar, E., Piran, T., & Sari, R. 2011, *ApJ*, 740, 100, doi: [10.1088/0004-637X/740/2/100](https://doi.org/10.1088/0004-637X/740/2/100)
- Caputo, R., Ajello, M., Kierans, C., et al. 2022, arXiv e-prints, arXiv:2208.04990, <https://arxiv.org/abs/2208.04990>
- Chodorowski, M. J., Zdziarski, A. A., & Sikora, M. 1992, *ApJ*, 400, 181, doi: [10.1086/171984](https://doi.org/10.1086/171984)
- Coward, D. M., Howell, E. J., Piran, T., et al. 2012, *MNRAS*, 425, 2668, doi: [10.1111/j.1365-2966.2012.21604.x](https://doi.org/10.1111/j.1365-2966.2012.21604.x)

- Dai, Z. G., & Lu, T. 1998, *A&A*, 333, L87.
<https://arxiv.org/abs/astro-ph/9810402>
- De Angelis, A., Tatischeff, V., Tavani, M., et al. 2017, *Experimental Astronomy*, 44, 25,
 doi: [10.1007/s10686-017-9533-6](https://doi.org/10.1007/s10686-017-9533-6)
- Dermer, C. D., Murase, K., & Takami, H. 2012, *ApJ*, 755, 147, doi: [10.1088/0004-637X/755/2/147](https://doi.org/10.1088/0004-637X/755/2/147)
- Ghirlanda, G., Salafia, O. S., Paragi, Z., et al. 2019, *Science*, 363, 968, doi: [10.1126/science.aau8815](https://doi.org/10.1126/science.aau8815)
- Gompertz, B. P., O'Brien, P. T., & Wynn, G. A. 2014, *MNRAS*, 438, 240, doi: [10.1093/mnras/stt2165](https://doi.org/10.1093/mnras/stt2165)
- Guetta, D., Hooper, D., Alvarez-Muniz, J., Halzen, F., & Reuveni, E. 2004, *Astroparticle Physics*, 20, 429,
 doi: [10.1016/S0927-6505\(03\)00211-1](https://doi.org/10.1016/S0927-6505(03)00211-1)
- Guo, F., Liu, Y.-H., Li, X., et al. 2020, *Physics of Plasmas*, 27, 080501, doi: [10.1063/5.0012094](https://doi.org/10.1063/5.0012094)
- Hamidani, H., & Ioka, K. 2021, *MNRAS*, 500, 627,
 doi: [10.1093/mnras/staa3276](https://doi.org/10.1093/mnras/staa3276)
- . 2022, arXiv e-prints, arXiv:2210.00814.
<https://arxiv.org/abs/2210.00814>
- Hamidani, H., Kiuchi, K., & Ioka, K. 2020, *MNRAS*, 491, 3192, doi: [10.1093/mnras/stz3231](https://doi.org/10.1093/mnras/stz3231)
- He, H.-N., Liu, R.-Y., Wang, X.-Y., et al. 2012, *ApJ*, 752, 29, doi: [10.1088/0004-637X/752/1/29](https://doi.org/10.1088/0004-637X/752/1/29)
- Hümmer, S., Baerwald, P., & Winter, W. 2012, *PhRvL*, 108, 231101, doi: [10.1103/PhysRevLett.108.231101](https://doi.org/10.1103/PhysRevLett.108.231101)
- Icecube Collaboration, Abbasi, R., Abdou, Y., et al. 2012, *Nature*, 484, 351, doi: [10.1038/nature11068](https://doi.org/10.1038/nature11068)
- IceCube Collaboration, Abbasi, R., Ackermann, M., et al. 2021, arXiv e-prints, arXiv:2101.09836.
<https://arxiv.org/abs/2101.09836>
- Ioka, K., Kobayashi, S., & Zhang, B. 2005, *ApJ*, 631, 429,
 doi: [10.1086/432567](https://doi.org/10.1086/432567)
- Kagawa, Y., Yonetoku, D., Sawano, T., et al. 2019, *ApJ*, 877, 147, doi: [10.3847/1538-4357/ab1bd6](https://doi.org/10.3847/1538-4357/ab1bd6)
- . 2015, *ApJ*, 811, 4, doi: [10.1088/0004-637X/811/1/4](https://doi.org/10.1088/0004-637X/811/1/4)
- Kaneko, Y., Bostanci, Z. F., Göğüş, E., & Lin, L. 2015, *MNRAS*, 452, 824, doi: [10.1093/mnras/stv1286](https://doi.org/10.1093/mnras/stv1286)
- Kasen, D., Metzger, B., Barnes, J., Quataert, E., & Ramirez-Ruiz, E. 2017, *Nature*, 551, 80,
 doi: [10.1038/nature24453](https://doi.org/10.1038/nature24453)
- Kasliwal, M. M., Nakar, E., Singer, L. P., et al. 2017, *Science*, 358, 1559, doi: [10.1126/science.aap9455](https://doi.org/10.1126/science.aap9455)
- Kimura, S. S. 2022, arXiv e-prints, arXiv:2202.06480.
<https://arxiv.org/abs/2202.06480>
- Kimura, S. S., Murase, K., Bartos, I., et al. 2018, *PhRvD*, 98, 043020, doi: [10.1103/PhysRevD.98.043020](https://doi.org/10.1103/PhysRevD.98.043020)
- Kimura, S. S., Murase, K., Ioka, K., et al. 2019, *ApJL*, 887, L16, doi: [10.3847/2041-8213/ab59e1](https://doi.org/10.3847/2041-8213/ab59e1)
- Kimura, S. S., Murase, K., Mészáros, P., & Kiuchi, K. 2017, *ApJL*, 848, L4, doi: [10.3847/2041-8213/aa8d14](https://doi.org/10.3847/2041-8213/aa8d14)
- Kisaka, S., & Ioka, K. 2015, *ApJL*, 804, L16,
 doi: [10.1088/2041-8205/804/1/L16](https://doi.org/10.1088/2041-8205/804/1/L16)
- Kisaka, S., Ioka, K., & Sakamoto, T. 2017, *ApJ*, 846, 142,
 doi: [10.3847/1538-4357/aa8775](https://doi.org/10.3847/1538-4357/aa8775)
- Kohri, K., Narayan, R., & Piran, T. 2005, *ApJ*, 629, 341,
 doi: [10.1086/431354](https://doi.org/10.1086/431354)
- Lamb, G. P., Lyman, J. D., Levan, A. J., et al. 2019, *ApJL*, 870, L15, doi: [10.3847/2041-8213/aaf96b](https://doi.org/10.3847/2041-8213/aaf96b)
- Levinson, A., & Eichler, D. 2003, *ApJL*, 594, L19,
 doi: [10.1086/378487](https://doi.org/10.1086/378487)
- Li, Z. 2012, *PhRvD*, 85, 027301,
 doi: [10.1103/PhysRevD.85.027301](https://doi.org/10.1103/PhysRevD.85.027301)
- Matsumoto, T., & Kimura, S. S. 2018, *ApJL*, 866, L16,
 doi: [10.3847/2041-8213/aae51b](https://doi.org/10.3847/2041-8213/aae51b)
- Mei, A., Banerjee, B., Oganessian, G., et al. 2022, *Nature*, 612, 236, doi: [10.1038/s41586-022-05404-7](https://doi.org/10.1038/s41586-022-05404-7)
- Metzger, B. D., Quataert, E., & Thompson, T. A. 2008, *MNRAS*, 385, 1455,
 doi: [10.1111/j.1365-2966.2008.12923.x](https://doi.org/10.1111/j.1365-2966.2008.12923.x)
- Moharana, R., & Piran, T. 2017, *MNRAS*, 472, L55,
 doi: [10.1093/mnrasl/slx131](https://doi.org/10.1093/mnrasl/slx131)
- Mooley, K. P., Nakar, E., Hotokezaka, K., et al. 2018a, *Nature*, 554, 207, doi: [10.1038/nature25452](https://doi.org/10.1038/nature25452)
- Mooley, K. P., Frail, D. A., Dobie, D., et al. 2018b, *ApJL*, 868, L11, doi: [10.3847/2041-8213/aaeda7](https://doi.org/10.3847/2041-8213/aaeda7)
- Murase, K., & Ioka, K. 2013, *PhRvL*, 111, 121102,
 doi: [10.1103/PhysRevLett.111.121102](https://doi.org/10.1103/PhysRevLett.111.121102)
- Murase, K., & Nagataki, S. 2006a, *PhRvD*, 73, 063002,
 doi: [10.1103/PhysRevD.73.063002](https://doi.org/10.1103/PhysRevD.73.063002)
- . 2006b, *PhRvL*, 97, 051101,
 doi: [10.1103/PhysRevLett.97.051101](https://doi.org/10.1103/PhysRevLett.97.051101)
- Murguia-Berthier, A., Ramirez-Ruiz, E., Kilpatrick, C. D., et al. 2017, *ApJL*, 848, L34,
 doi: [10.3847/2041-8213/aa91b3](https://doi.org/10.3847/2041-8213/aa91b3)
- Norris, J. P., & Bonnell, J. T. 2006, *ApJ*, 643, 266,
 doi: [10.1086/502796](https://doi.org/10.1086/502796)
- Perna, R., Armitage, P. J., & Zhang, B. 2006, *ApJL*, 636, L29, doi: [10.1086/499775](https://doi.org/10.1086/499775)
- Rastinejad, J. C., Gompertz, B. P., Levan, A. J., et al. 2022, *Nature*, 612, 223, doi: [10.1038/s41586-022-05390-w](https://doi.org/10.1038/s41586-022-05390-w)
- Rees, M. J., & Mészáros, P. 2005, *ApJ*, 628, 847,
 doi: [10.1086/430818](https://doi.org/10.1086/430818)
- Rouco Escorial, A., Fong, W.-f., Berger, E., et al. 2022, arXiv e-prints, arXiv:2210.05695.
<https://arxiv.org/abs/2210.05695>
- Rowlinson, A., O'Brien, P. T., Metzger, B. D., Tanvir, N. R., & Levan, A. J. 2013, *MNRAS*, 430, 1061,
 doi: [10.1093/mnras/sts683](https://doi.org/10.1093/mnras/sts683)

- Sakamoto, T., Barthelmy, S. D., Baumgartner, W. H., et al. 2011, *ApJS*, 195, 2, doi: [10.1088/0067-0049/195/1/2](https://doi.org/10.1088/0067-0049/195/1/2)
- Sarin, N., Lasky, P. D., Vivanco, F. H., et al. 2022, *PhRvD*, 105, 083004, doi: [10.1103/PhysRevD.105.083004](https://doi.org/10.1103/PhysRevD.105.083004)
- Shibata, M., Fujibayashi, S., Hotokezaka, K., et al. 2017, *PhRvD*, 96, 123012, doi: [10.1103/PhysRevD.96.123012](https://doi.org/10.1103/PhysRevD.96.123012)
- Stepney, S., & Guilbert, P. W. 1983, *MNRAS*, 204, 1269, doi: [10.1093/mnras/204.4.1269](https://doi.org/10.1093/mnras/204.4.1269)
- Tanaka, M., Utsumi, Y., Mazzali, P. A., et al. 2017, *PASJ*, 69, 102, doi: [10.1093/pasj/psx121](https://doi.org/10.1093/pasj/psx121)
- Toma, K., Wu, X.-F., & Mészáros, P. 2009, *ApJ*, 707, 1404, doi: [10.1088/0004-637X/707/2/1404](https://doi.org/10.1088/0004-637X/707/2/1404)
- Troja, E., Piro, L., Ryan, G., et al. 2018, *MNRAS*, 478, L18, doi: [10.1093/mnrasl/sly061](https://doi.org/10.1093/mnrasl/sly061)
- Troja, E., Fryer, C. L., O'Connor, B., et al. 2022, *Nature*, 612, 228, doi: [10.1038/s41586-022-05327-3](https://doi.org/10.1038/s41586-022-05327-3)
- Wanderman, D., & Piran, T. 2015, *MNRAS*, 448, 3026, doi: [10.1093/mnras/stv123](https://doi.org/10.1093/mnras/stv123)
- Waxman, E., & Bahcall, J. 1997, *PhRvL*, 78, 2292, doi: [10.1103/PhysRevLett.78.2292](https://doi.org/10.1103/PhysRevLett.78.2292)
- . 1998, *PhRvD*, 59, 023002, doi: [10.1103/PhysRevD.59.023002](https://doi.org/10.1103/PhysRevD.59.023002)
- Xue, Y. Q., Zheng, X. C., Li, Y., et al. 2019, *Nature*, 568, 198, doi: [10.1038/s41586-019-1079-5](https://doi.org/10.1038/s41586-019-1079-5)
- Yang, J., Ai, S., Zhang, B.-B., et al. 2022, *Nature*, 612, 232, doi: [10.1038/s41586-022-05403-8](https://doi.org/10.1038/s41586-022-05403-8)
- Ye, Z. P., Hu, F., Tian, W., et al. 2022, arXiv e-prints, arXiv:2207.04519. <https://arxiv.org/abs/2207.04519>
- Zhang, B., & Kumar, P. 2013, *PhRvL*, 110, 121101, doi: [10.1103/PhysRevLett.110.121101](https://doi.org/10.1103/PhysRevLett.110.121101)
- Zhang, B., & Yan, H. 2011, *ApJ*, 726, 90, doi: [10.1088/0004-637X/726/2/90](https://doi.org/10.1088/0004-637X/726/2/90)
- Zhang, H.-M., Huang, Y.-Y., Zheng, J.-H., Liu, R.-Y., & Wang, X.-Y. 2022, *ApJL*, 933, L22, doi: [10.3847/2041-8213/ac7b23](https://doi.org/10.3847/2041-8213/ac7b23)